Takano, J. Tang, Y. Lin and M. Tachibana, "Structural characterization of the C60 nanowhiskers heat-treated at high temperatures for potential superconductor application", Trans. Mat. Res. Soc. Japan, 38[4](2013)517-520

2. 学会発表

(1) 今野俊生，若原孝次，宮澤薫一，"C_{60}-C_{70}2 成分ナノウィスカーの合成"，ナノファイバー学会第 4 回年次大会講演予稿集,P.26, 2013 年 7 月 5 日，つくば

(2) D. Matsuura, C. Hirata, T.Konno, T.Wakahara, K. Miyazawa, T. Kizuka, " In Situ Transmission Electron Microscopy of Bending Process of C_{60}/C_{70} Nanowhiskers", Abstracts of APPC12, The 12th Asia Pacific Physics Conference, pp. 865-865, 2013 年 7 月 14-19 日,千葉

(3) T. Konno, T.Wakahara and K. Miyazawa, "Synthesis and Structural Analyses of C_{60}-C_{70} Two-Component Fullerene Nanowhiskers", Abstracts of 23rd Annual Meeting of MRS-Japan 2013, P.J-O9-006, Dec. 9-11, 2013, Yokohama Port Opening Plaza, Yokohama

(4) Kun'ichi Miyazawa, Chika Hirata, Toshio Konno, Takatsugu Wakahara, Ryosuke Kano,Masaru Tachibana, "Synthesis of C_{60}-C_{70} two-component fullerene nanowhiskers by LLIP method", nanoeh6abs program, P.28-28, 6th International Symposium on Nanotechnology, Occupational and Environmental Health, Nagoya Congress Center, October 28 - 31, 2013, Nagoya

(5) 今野俊生，若原孝次，宮澤薫一，"C_{60}-C_{70}2 成分ナノウィスカーの合成と構造解析"，日本物理学会講演概要集，第 68 巻第 2 号第 4 分冊，P.740, 2013 年秋季大会，2013 年 9 月 25 日～9 月 28 日，徳島

(6) 松浦大輔，今野俊生，若原孝次，宮澤薫一，木塚徳志，"C_{60}/C_{70}合金ナノウィスカーのヤング率の組成依存性"，2014 年春期講演大会（第 154 回）日本金属学会講演大会概要集，P.22, 2014 年 3 月 21 日～23 日，東京

H. 知的財産権の出願・登録状況

1. なし
2. 実用新案登録
   (該当なし)
3. その他
   (該当なし)

平成 25 年度　厚生労働科学研究費補助金（化学物質リスク研究事業）分担研究報告書

研究課題名：ナノマテリアル曝露による生体毒性の慢性移行及び遅発性に関わる
評価手法の開発研究

分担研究課題名：ナノマテリアルの慢性影響および生殖発生毒性評価系に関する研究

研究分担者：広瀬　明彦　　国立医薬品食品衛生研究所総合評価研究室　室長
研究協力者：小縣　昭夫　　東京都健康安全研究センター　薬事環境科学部　主任研究員
　　　　　　坂本　義光　　東京都健康安全研究センター　薬事環境科学部　主任
　　　　　　山本　行男　　東京都健康安全研究センター　薬事環境科学部　主任
　　　　　　藤谷　知子　　東京都健康安全研究センター　薬事環境科学部　主任
　　　　　　北條　幹　　　東京都健康安全研究センター　薬事環境科学部　主任
　　　　　　猪又　明子　　東京都健康安全研究センター　薬事環境科学部　科長
　　　　　　中江　大　　　東京都健康安全研究センター　薬事環境科学部　部長
　　　　　　西村　哲治　　帝京平成大学薬学部薬学科　教授
　　　　　　平田　睦子　　国立医薬品食品衛生研究所　総合評価研究室　主任研究員
　　　　　　小野　敦　　　国立医薬品食品衛生研究所　総合評価研究室　主任研究員
　　　　　　高橋　美加　　国立医薬品食品衛生研究所　総合評価研究室　研究員
　　　　　　松本　真理子　国立医薬品食品衛生研究所　総合評価研究室　研究員
　　　　　　加藤　日奈　　国立医薬品食品衛生研究所　総合評価研究室　研究員
　　　　　　川村　智子　　国立医薬品食品衛生研究所　総合評価研究室　研究員
　　　　　　小林　克己　　国立医薬品食品衛生研究所　総合評価研究室　研究員
　　　　　　江馬　眞　　　国立医薬品食品衛生研究所　客員研究員

研究要旨

　本研究では、ナノマテリアル曝露による生体毒性の慢性移行及び遅発性に関わる研究の一環として、多層カーボンナノチューブ(MWCNT)の腹腔内投与および気管内投与による中皮腫誘発性につい繊維長が及ぼす影響、MWCNT により誘発されたラット中皮腫のプロテオーム解析および、ナノマテリアルの催奇形性について解析を行っている。25年度は、経気管反復投与においても誘発率としては弱いものの MWCNT が中皮腫誘発性を示すことを確認した。また、投与した試料の繊維長の解析からは、気管内投与による中皮腫誘発性にも繊維長が関連していることが示唆された。また、中皮腫誘発性の高い形状を持つ MWCNT の方が、誘発率の弱いものに比べて血清中のタンパク質の発現変動に与える影響も大きいことが、プロテオーム解析から検証された。しかし、そこで発現するタンパク質と中皮腫との関連性についてはさらなる検討は必要である。一方、多層カーボンナノチューブに形状が類似しているアスベストについても CNT の 10 倍量の大量投与により催奇形性作用を示すことが確認され、奇形発現要因の一つとしても繊維本数や繊維長との関連性のあることが示唆された。

A．研究目的

　近年、新素材である産業用ナノマテリアルは、新たな用途や特性をもたらすと期待されている物理化学特性により、ヒト健康にも未知の影響を及ぼす可能性が指摘されているが、そのための適切な健康リスク評価を行えるほどの知見は未だ

十分に集積したとは言えない。この問題は 2004 年頃から現在まで国内外共に社会的な関心として高い状態である。国際機関においても OECD が 2006 年から産業用ナノマテリアルの作業グループを設置し、有害性情報の収集、評価に対してスポンサーシッププログラムを中心とした活動が行なわれている。このプログラムでは、現在までに得られた情報を整理すると共に、更なる知見の必要性やガイドラインの見直し等の検討が行われているところである。我々のこれまでの研究では、その研究開始当初より体内残留性に基づいた慢性影響が最も懸念すべき健康影響であるとの認識に則り、特にアスベスト様形状を持つ多層型カーボンナノチューブ（MWCNT）については中皮腫を誘発するポテンシャルを持つことを明らかにしてきた。さらに、我々は MWCNT の曝露が催奇形性ポテンシャルを持つことも平成 23 年度の研究で明らかにした。25 年度は MWCNT による気管内投与による慢性影響と中皮腫誘発時におけるプロテオーム解析、及び催奇形性誘発関するアスベストとの類似性に関する研究を行うことを目的とした。

B．研究方法

1．多層カーボンナノチューブのラットによる経気管反復投与及び投与後 52 週間飼育実験

ヒトへのばく露条件を考慮した経気管反復投与及び投与終了後長期飼育による多層カーボンナノチューブ（MWCNT）のラット呼吸器系への影響を観察した。動物は, RccHan™:WIST 系, 雄性ラット 10 週齢を用いた. MWCNT は, M 社製 MWCNT-7[長さ 2 μm, 径 75 nm, Fe 含有量 0.344%]を分散液に懸濁し, 0.01（L 群）, 0.05（M 群）及び 0.25 mg/kg 体重(H 群)の用量で, 各群 20 匹に, 1 回/4 週間, 計 12 回, 経気管噴霧投与した. 分散液の調整は MWCNT の 20 倍量のショ糖でらい解した後、さらに 20 倍量の Tween 80 を加え、らい解した後、イオン交換水で MWCNT 濃度として 0.25%になるよう調整した（特許公開 2008-230935）。動物は、投与後 52 週間を目処に飼育し, 終了時生存例について, 病理学的に検索した.

2．多層カーボンナノチューブ（MWCNT）により誘発されたラット中皮腫のプロテオーム解析

MWCNT 投与実験：F344（12 週令，n=10））の腹腔内に形状の異なる MWCNT（S 社製 SD-1: L= 8 μm, ϕ = 150 nm ; SD-2: L= 3 μm, ϕ = 10-15 nm) を単回投与（1.0mg/kg）後、50 週前後で血液を採取し血清に分離した。

二次元電気泳動による発現差異解析および LC/MS/MS による有意変動タンパク質の同定：血清サンプルは前処理により、アルブミンと IgG を分離除去した。次いで、サンプル（対照群， SD-1 投与群、SD-2 投与群）各 25 μg を蛍光色素（Cy2, Cy3, Cy5: 各 200 pmol/25 μg ）で標識した。標識サンプルは、蛍光ディフェレンスゲル二次元電気泳動法（2 D-DIGE）に従い、等電点電気泳動そして SDS 電気泳動を行なった。二次元に分離展開したタンパク質スポットの画像を取り込み 、DeCyder 解析ソフトを用いて発現スポットの検出、マッチング、有意差検定を行った。得られた有意スポットをトリプシン消化後、LC/MS/MS 法にて分析し、候補タンパク質を同定した。

3．多層カーボンナノチューブ類似物質としてのアスベストの催奇形性（腹腔内投与）

UICC のアスベスト（クロシドライト、クリソタイルおよびアモサイト）を 2%カルボキシメチルセルロースナトリウム（東京化成工業）/りん酸緩衝生理食塩水を用いて、磁気端子攪拌機および超音波処理により懸濁した後、高圧蒸気滅菌し、妊娠 9 日目の CD1 マウスに 4mg あるいは 40mg/kg 体重を腹腔内投与した。妊娠 18 日に胎仔の外表奇形と骨格奇形を検査した。

C．研究結果

1．多層カーボンナノチューブのラットによる経気管反復投与及び投与後 52 週間飼育実験

投与期間中の途中死亡例, 瀕死例の発現, 終了時生存例の一般症状及び体重増加推移に投与と関連した異常は認められなかった. 終了時生存例について, 組織学的に, MWCNT の沈着は, 主にマクロファージに貪食された状態で肺胞内, 細気管支や血管壁周囲のリンパ組織内に認められた. 最終投与終

了後 52 週目の MWCNT の肺内沈着量は、L,M 群に比べて、H 群で顕著に多かった. また肺の呼吸細気管支, 肺胞管及び肺胞における, 末梢性の増殖性病変が認められた(表 1)。中皮組織の組織学的変化では、M 及び H 群で腹腔内中皮腫各1例が、また H 群に心嚢膜中皮腫が 1 例、臓側胸膜中皮細胞の肥大及び過形成が夫々1例ずつ観察された(表2)。

2. 多層カーボンナノチューブ(MWCNT)により誘発されたラット中皮腫のプロテオーム解析

血清サンプルの発現差異解析は、各群6サンプルずつ2回行った。本解析では、マスターゲル上で951ヶのタンパク質スポットを検出した。対照群に対する投与群のサンプルにおける発現量の変化は、T 検定(p<0.05)において SD-1 投与群が 5.3%、SD-2 投与群が 3.7%の有意変動を認めた。また、2倍以上の発現量比を示すものは、SD-1 投与群が 17.9%と SD-2 投与群が 12%であった。更に両方の条件を満たすものは、それぞれ 20 ヶと 9 ヶのタンパク質が認められた (表3)。これらのスポットのうち、発現変動の影響が大きい SD-1 投与群の6ヶについて、LC/MS/MS による同定を行った。その結果、タンパク質分解の調節作用、酸化酵素、ヘムタンパク質の結合調節作用、リポタンパク質の運搬作用を持つタンパク質が同定され、現在、確認作業を行っている(表4)。

3. 多層カーボンナノチューブ類似物質としてのアスベストの催奇形性 (腹腔内投与)

クロシドライト、クリソタイルおよびアモサイトの 4mg/kg 体重の投与では、母体あたりの, 総着床数と, 早期死胚数, 後期死胚数, 生存胎仔数およびそれらの総着床数中の%, 生存胎仔総重量および胎仔の平均重量 (雌雄) は, 対照群と各投与群間で有意差はなかった。クロシドライト投与群で外脳と多指がそれぞれ1例ずつ、アモサイト投与群で眼瞼開裂が1例見られたが、その発現頻度は、対照群と有意差はなかった(表5)。

しかし、投与量 40mg/kg 体重では、クロシドライト投与群で着床数中の生存胎仔の割合 (%) が有意に低下し、クリソタイル投与群およびアモサイト投与群で早期死胚を有する母体の頻度が有意に増加した。また、アモサイト投与群で四肢減形成を主とする外表奇形および脊柱の癒合・四肢減形成を主とする骨格奇形が、クロシドライト投与群およびクリソタイル投与群で脊柱の癒合を主とする骨格奇形が有意に発現した (表6)。

D. 考察

気管内投与で認められた中皮細胞の増殖性病変としては, 0.05 及び 0.25 mg/kg 群で腹腔内中皮腫、0.25mg/kg 群で心嚢膜の中皮腫、臓側胸膜の中皮細胞の過形成及び肥大が認められたが、いずれも発現率が低かった。また MWCNT 投与群における肺実質及び胸膜における腫瘍の発現は認められなかった。ラットに経気管投与した MWCNT は肺の増殖性病変と低頻度ながら中皮種を誘発する可能性を示したが, その生物学的意義については現在なお検討中である。

今回の MWCNT の経気管反復投与実験において、経気管投与用に調製した分散液中の MWCNT-7 繊維サイズの分布は、繊維長が 1-4μm 以下が 95.8%、5μm 以上が 4.2%と既報の腹腔内投与に用いた MWCNT より繊維長の短いものであったが、この試料を 0.25 mg/kg で腹腔内単回投与した場合の腹膜中皮腫の発現率は 4/20 例(20%)であった。尚、参考データとして表 2 に示したように、MWCNT-7 の 2%CMC で懸濁液を 0.1 及び 0.3mg/kg 体重で単回腹腔内投与し約 52 週後の中皮腫発生率は 64-83%であることから、今回の試験で呼吸器系上皮及び体腔膜上皮の反応が想定される反応より、弱かった理由としては、投与試料とした MWCNT のサイズが短かった可能性がある。しかし、この経気管投与のための試料でも中皮腫誘発性を有することが確認された。

中皮腫誘発性に関する血清中蛋白の発現差異解析から、長さおよび径の相対的に大きな構造をもつ SD-1 投与が、小さな構造を持つ SD-2 投与に比較して、血清中のタンパク質の発現変動に与える影響が大きかった。このことは、MWCNT のラット投与後 50 週前後で、結節や中皮腫などの病理組織所見に認められるように全身性の病態変化を引き起こし、投与部位から血液循環系へ影響が

波及した結果と考えられる。現在、LC/MS/MS の結果から同定されたタンパク質は、中皮腫発症との関連性について解っておらず今後の課題となっている。今後、病理組織所見による結節および中皮腫の発現がある病変組織をサンプルとして、解析を進めていくことが重要と考えられる。

多層カーボンナノチューブ類似物質として試験した３種のアスベスト（クロシドライト、クリソタイルおよびアモサイト）の 40mg/kg 体重の腹腔内投与でも、H23 年に報告した M 社製 MWCNT-7 や H24 年に報告した N 社製 MWCNT を投与した実験と同様の奇形が認められた、その発現用量は MWCNT に比べると、はるかに高用量によるものであった。しかしながら、今回の試験によりアスベストにも催奇形性作用のあることが確認されると共に、M 社製 MWCNT や N 社製 MWCNT との発現する奇形の類似性を考えると、奇形発現要因の一つには繊維本数や繊維長との関連も示唆された。今後は、繊維長や分散性の異なる CNT においても検討を加えていく必要があると考えられた。

E．結論

今回の研究では、経気管反復投与においても誘発率としては弱いものの MWCNT が中皮腫誘発性を示すことを実証した。また、投与した試料の繊維長の解析からは、気管内投与による中皮腫誘発性にも繊維長が関連していることが示唆された。また、中皮腫誘発性の高い形状を持つ MWCNT の方が、誘発率の弱いものに比べて血清中のタンパク質の発現変動に与える影響も大きいことが、プロテオーム解析から検証された。しかし、そこで発現するタンパク質と中皮腫との関連性についてはさらなる検討は必要である。一方、多層カーボンナノチューブに形状が類似しているアスベストについても CNT の 10 倍量の大量投与により催奇形性作用を示すことが確認され、奇形発現要因の一つにも繊維本数や繊維長との関連性のあることが示唆された。

F．健康危機情報

該当無し

G．研究発表

（論文発表）

Xu J, Futakuchi M, Alexander DB, Fukamachi K, Numano T, Suzui M, Shimizu H, Omori T, Kanno J, Hirose A, Tsuda H. Nanosized zinc oxide particles do not promote DHPN-induced lung carcinogenesis but cause reversible epithelial hyperplasia of terminal bronchioles. Arch Toxicol. 88:65–75. (2014)

Taquahashi, Y, Ogawa, Y, Takagi, A, Tsuji, M, Morita, K, Kanno, J. An improved dispersion method of multi-wall carbon nanotube for inhalation toxicity studies of experimental animals. J Toxicol Sci. 38(4):619-28. (2013)

Numano T1, Xu J, Futakuchi M, Fukamachi K, Alexander DB, Furukawa F, Kanno J, Hirose A, Tsuda H, Suzui M. Comparative study of toxic effects of anatase and rutile type nanosized titanium dioxide particles in vivo and in vitro. Asian Pac J Cancer Prev. 15(2):929-935. (2014)

広瀬明彦, ナノマテリアルの健康影響評価指針の国際動向, 薬学雑誌, 133(2), 175-180. (2013)

（学会発表）

Akihiko Hirose, Norihiro Kobayashi, Tomoko Fujitani, Yoshimitsu Sakamoto, Yasuo Yoshioka, Yasuo Tsutsumi, Hiroyuki Tsuda, Jun Kanno : Nanotoxicity and nano safety science in various exposure scenarios. (Symposium invited) EUROTOX2013 (2013.9, Switzerland, Interlaken)

Akihiko Hirose, Norihiro Kobayashi, Mayumi Kawabe*1, Hironao Nakashima*1, Takamasa Numano*1*2, Reiji Kubota, Yoshiaki Ikarashi: Developmental toxicity by intratracheal instillation of multi-wall carbon nanotubes in pregnant mice. 6th International Symposium Nanotechnology, Ocupational and Environmental Health (2013.10, Nagoya)

坂本義光, 小縣昭夫, 湯澤勝弘、久保喜一、安藤弘、長澤明道、高橋博、矢野範男、西村哲治, 広瀬明彦, 井上義之、橋爪直樹、猪又明子、中江 大 "ラットにおいて多層カーボンナノチューブの経気管噴霧反復投与が及ぼす影響" 第30回 日本毒性病理学会 2014. 1. 徳島

坂本義光, 小縣昭夫, 猪又明子, 西村哲治, 広瀬明彦, 中江 大 "繊維長の異なる多層カーボンナノチューブによるラット中皮腫誘発性の検討" 第40回日本毒性学会 2013.6, 幕張

藤谷知子、安藤弘、久保喜一、猪又明子、小縣昭夫、広瀬明彦、西村哲治、中江大：マウスにおけるナノマテリアルの催奇形性に関する研究。第40回日本毒性学会学術年会、2013, 6,17-19, 幕張

小林憲弘、沼野琢旬、中島弘尚、河部真弓、久保田領志、広瀬明彦：妊娠マウスを用いた気管内投与による多層カーボンナノチューブの生殖・発生毒性の評価、第40回日本毒性学会学術年会、2013, 6,17-19, 幕張

山本行男、坂本義光、大貫文、猪又明子、小縣昭夫、広瀬明彦、中江大：多層カーボンナノチューブ（MWCNT）投与による中皮腫誘発ラットにおけるプロテオーム解析 (第三報)：形状の異なるMWCNT投与ラットにおける血清タンパク質の発現変動。第86回日本生化学会大会、2013, 9,11-13, 横浜

Sakamoto Y, Ogata A, Nishimura T, Hirose A, Nakae D.Induction of mesothelioma by an intraperitoneal administration of 7 different manufactured multi-wall carbon nanotubes.72 th Annual Meeting of the Japanese Cancer Association ; Yokohama, 2013,10

Nishimaki-Mogami, T., Cui, H., Wu, W., Okuhira, K., Naito, M., Nishimura, T., Sakamoto, Y., Ogata, A., Maeno, T., Inomata, A., Nakae, D., Miyazawa, K., Hirose, A. High-temperature calcined fullerene nanowhiskers and multi-wall carbon nanotubes have abilities to induce IL-1beta secretion through NLRP3-dependent mechanism, depending on their lengths. EUROTOX 2013 (9.3) (Interlaken, Switzerland)

H. 知的財産権の出願・登録状況（予定を含む）
1. 特許取得
    （該当なし）
2. 実用新案登録
    （該当なし）
3. その他
（該当なし）

表1 呼吸器系組織所見

実験群/用量 (mg/kg)	観察例数	泡沫細胞集簇	炎症	線維化	増殖性病変			
					細気管支	終末細気管支－肺胞		肺胞領域細気管支/肺胞上皮細胞
					非線毛性	非線毛性	線毛性	
対照群(分散液)	18	4 (22)	4 (22)	6 (35)	2 (11)	1 (6)	1 (6)	0
0.01	15	2 (13)	3 (20)	4 (56)	5 (33)	2 (13)	1 (7)	0
0.05	16	4 (25)	6 (40)	8 (52)	6 (40)	3 (19)	3 (19)	0
0.25	15	5 (37)	12 (82)*	14 (98)*	4 (29)	4 (29)	5 (33)	7(48)*

( )内%

神経内分泌細胞過形成　細気管支上皮化　肺胞上皮過形成
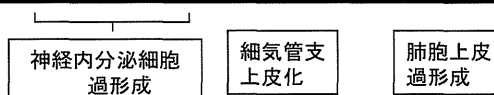
表2 中皮細胞増殖性病変

実験群/用量 (mg/kg)	観察例数	肉眼所見 腫瘍結節 出血性体液			組織所見								
		心膜	胸膜	腹膜	心膜			胸膜			腹膜		
					肥大	過形成	中皮腫	肥大	過形成	中皮腫	肥大	過形成	中皮腫
気管内投与群													
対照群	19	0	0	0	0	0	0	0	0	0	0	0	0
0.01	16	0	0	0	0	0	0	0	0	0	0	0	0
0.05	20	0	0	1	0	0	0	0	0	0	0	0	1(5%)
0.25	17	0	0	0	0	0	1(6%)	1	1	0	0	0	1(6%)
腹腔内投与群													
対照群	19	0	0	0	0	0	0	0	0	0	0	0	0
0.25	20	0	0	1	0	0	0	0	0	0	7	1	4 (20%)
(参考データ:既報の試料による腹腔内投与実験)													
0.1	11												7 (64%)
0.3	12												10 (83%)

表3　　プレ手オーム発現差異解析の結果

グループ	検出スポット数	T検定（P<0.05）（A）スポット数	発現量比（2倍の増減）（B）スポット数	(A)&(B)
SD-1	951	50（5.3%）	167（16.7%）	20（2.1%）
SD-2	951	35（3.7%）	114（12.0%）	9（0.9%）

検出スポット数はマスターゲル上の数を示す。（A）コントロールに対する発現強度のT検定では、　SD-1投与群とSD-2投与群では、5.3%と3.7%と有意の変動が得られた。（B）2倍以上の発現量比を　示すものは、SD-1投与群で16.7%、一方、SD-2投与群で12%だった。　有意かつ2倍以上の変動を　示すものとしては、各群それぞれで2.1%と0.9%であった。

表4　　有意の発現差異を示すスポット（対照群とSD-1投与群間）のMS/MSデータ

ID番号	タンパク質名	分子量	等電点	マッチ数	回収率(%)	PGDSスコア
P14046	α-1 inhibitor III	163669	5.63	6	5.7	133.1
P13635	Ceruloplasmin EC 1 16 3 1	120763	5.22	5	4.8	176.8
P04639	Apolipoprotein A-IV	44428	4.94	4	12.4	279.1
P06866	Haptoglobin	38524	6.09	2	18.7	163.1

LC/MS/MS分析は、Ｗａｔｅｒｓ社のnano-Ａｃｑｕｉｔｙ-Synaptを用いて行った。
マッチ数は、トリプシン消化後のペプチドの数を示し、回収率は、全配列に対する回収したペプチドの割合を示す。
PGDSスコアは、同定に対する信頼性を示す数値で、50より大きい数値ほど信頼性が高い。

表5　アスベスト4mg/kg体重の腹腔内投与の影響

		対照群	クロシドライト	クリソタイル	アモサイト
母体数		9	10	10	10
体重	投与時	39.0±1.9	35.8±4.2	36.3±2.8	37.0±3.2
	最終	70.2±6.0	65.0±2.0	66.7±8.3	65.3±7.8
黄体数		16.8±1.5	16.6±1.5	16.7±1.3	16.5±1.8
着床数		16.0±2.1	14.6±1.6	145.1±2.3	15.2±2.3
吸収胚	早期（数/母体）	1.0±0.7	0.3±0.5	0.6±0.7	1.5±2.5
	後期（数/母体）	0±0	0.3±0.5	0.1±0.3	0.1±0.3
生存胎仔数		15.0±2.4	14.0±1.6	14.2±2.5	13.6±3.5
生存胎仔平均重量	雄	1.45±0.09	1.45±0.08	1.45±0.08	1.49±0.06
	雌	1.40±0.08	1.37±0.08	1.39±0.06	1.41±0.06
外表奇形を有した母体数		0	2	0	1
外表奇形を有した胎仔数/全胎仔数		0/135	2/140	0/142	1/136
観察された奇形			外脳・眼瞼開裂・多指		眼瞼開裂
骨格奇形を有した母体数		0	2	0	0
骨格奇形を有した胎仔数/全胎仔数		0/135	2/140	0/142	0/136
観察された奇形			頭骨形成不全・多指		

数値は、母体毎の平均値±標準偏差、あるいは、観察された頻度。

表 6　アスベスト 40mg/kg 体重の腹腔内投与の影響

		対照群	クロシドライト	クリソタイル	アモサイト
母体数		9	10	9	10
体重	投与時	37.5±2.1	37.9±1.1	36.6±1.8	37.6±2.0
	最終	67.0±6.0	59.5±8.7	60.0±6.9	65.1±8.2
黄体数		17.9±1.8	19.3±1.3	18.7±1.3	18.5±1.4
着床数		14.6±2.5	14.4±1.6	14.2±1.2	14.9±1.4
吸収胚	早期(数/母体)	0.1±0.3	5.1±5.5	3.9±4.3	3.2±3.3
	（吸収胚を有する母体数）	1	5	8**	8**
	後期(数/母体)	0±0	0.2±0.4	0±0	0.1±0.3
生存胎仔数		14.4±2.7	9.2±5.3	10.3±3.9	11.6±3.7
生存胎仔平均重量	雄	1.47±0.08	1.42±0.12	1.43±0.04	1.40±0.08
	雌	1.39±0.08	1.33±0.09	1.35±0.06	1.33±0.08
外表奇形を有した母体数		0	1	1	4*
外表奇形を有した胎仔数/全胎仔数		0/130	1/92	1/93	5/116*
観察された奇形			少指	眼瞼開裂	少指、顔面裂、無尾
骨格奇形を有した母体数		0	3	4*	7**
骨格奇形を有した胎仔数/全胎仔数		0/130	6/92*	5/93*	13/116***
観察された奇形			少指・脊椎癒合	脊椎癒合・肋骨癒合	少指・脊椎癒合・肋骨癒合

数値は、母体毎の平均値±標準偏差、あるいは、観察された頻度。

Ⅲ．研究成果の刊行に関する一覧表

書籍

著者名	論文タイトル	書籍全体の編集者名	書籍名	出版社名	出版地	出版年	ページ

雑誌

著者名	論文タイトル	発表誌名	巻号	ページ	出版年
Numano T, Xu J, Futakuchi M, Fukamachi K, Alexander DB, Furukawa F, Kanno J, Hirose A, Tsuda H, Suzui M.	Comparative Study of Toxic Effects of Anatase and Rutile Type Nanosized Titanium Dioxide Particles in vivo and in vitro.	sian Pac J Cancer Prev.	15(2)	929-35	2014
Xu J, Futakuchi M, Alexander DB, Fukamachi K, Numano T, Suzui M, Shimizu H, Omori T, Kanno J, Hirose A, Tsuda H	Nanosized zinc oxide particles do not promote DHPN-induced lung carcinogenesis but cause reversible epithelial hyperplasia of terminal bronchioles.	Arch Toxicol.	88	65-75	2014 Jan
Taquahashi, Y, Ogawa, Y, Takagi, A, Tsuji, M, Morita, K, Kanno, J.	An improved dispersion method of multi-wall carbon nanotube for inhalation toxicity studies of experimental animals.	J Toxicol Sci.	38(4)	619-28	2013
Ohba T., Sagawa E., Suzuki Y., Yamamura H., Ohya S., Tsuda H., and Imaizumi Y.	Enhancement of Ca2＋ Influx and Ciliary Beating by Membrane Hyperpolarization due to ATP-Sensitive K+ Channel Opening in Mouse Airway Epithelial Cells	J Pharmacol Exp Ther	347	145-153	2013
Kumiko Shimizu, Reiji Kubota, Norihiro Kobayashi, Maiko Tahara, Naoki Sugimoto, Tetsuji	Cytotoxic Effects of Hydroxylated Fullerenes in Three Types of Liver Cells	Materials	6(7)	2713-2722	2013

Nishimura, Yoshiaki Ikarashi					
Stefan Pfuhler, Rosalie Elespuru, Marilyn Aardema, Shareen H. Doak, E. Maria Donner, Masamitsu Honma, Micheline Kirsch-Volders, Robert Landsiedel, Mugimane Manjanatha, Tim Singer, James H. Kim	Genotoxicity ofNanomaterials: Refining Strategies and Tests for Hazard Identification	Environment Mol. Mutagen.	54	229-239	2013
K. Miyazawa, C. Hirata, R. Kano, T. Wakahara, H. Takeya, T. Yamaguchi,Y. Takano, J. Tang, Y. Lin and M. Tachibana	Structural characterization of the C60 nanowhiskers heat-treated at high temperatures for potential superconductor application	Trans. Mat. Res. Soc. Japan	38[4]	517-520	2013
広瀬明彦	ナノマテリアルの健康影響評価指針の国際動向	薬学雑誌	133 (2)	175-180	2013

IV. 研究成果の刊行物・別冊

RESEARCH ARTICLE

Comparative Study of Toxic Effects of Anatase and Rutile Type Nanosized Titanium Dioxide Particles *in vivo* and *in vitro*

Takamasa Numano[1,3], Jiegou Xu[2], Mitsuru Futakuchi[1], Katsumi Fukamachi[1], David B Alexander[2], Fumio Furukawa[3], Jun Kanno[4], Akihiko Hirose[4], Hiroyuki Tsuda[2], Masumi Suzui[1]*

Abstract

Two types of nanosized titanium dioxide, anatase (anTiO$_2$) and rutile (rnTiO$_2$), are widely used in industry, commercial products and biosystems. TiO$_2$ has been evaluated as a Group 2B carcinogen. Previous reports indicated that anTiO$_2$ is less toxic than rnTiO$_2$, however, under ultraviolet irradiation anTiO$_2$ is more toxic than rnTiO$_2$ *in vitro* because of differences in their crystal structures. In the present study, we compared the *in vivo* and *in vitro* toxic effects induced by anTiO$_2$ and rnTiO$_2$. Female SD rats were treated with 500 µg/ml of anTiO$_2$ or rnTiO$_2$ suspensions by intra-pulmonary spraying 8 times over a two week period. In the lung, treatment with anTiO$_2$ or rnTiO$_2$ increased alveolar macrophage numbers and levels of 8-hydroxydeoxyguanosine (8-OHdG); these increases tended to be lower in the anTiO$_2$ treated group compared to the rnTiO$_2$ treated group. Expression of MIP1α mRNA and protein in lung tissues treated with anTiO$_2$ and rnTiO$_2$ was also significantly up-regulated, with MIP1α mRNA and protein expression significantly lower in the anTiO$_2$ group than in the rnTiO$_2$ group. In cell culture of primary alveolar macrophages (PAM) treated with anTiO$_2$ and rnTiO$_2$, expression of MIP1α mRNA in the PAM and protein in the culture media was significantly higher than in control cultures. Similarly to the *in vivo* results, MIP1α mRNA and protein expression was significantly lower in the anTiO$_2$ treated cultures compared to the rnTiO$_2$ treated cultures. Furthermore, conditioned cell culture media from PAM cultures treated with anTiO$_2$ had less effect on A549 cell proliferation compared to conditioned media from cultures treated with rnTiO$_2$. However, no significant difference was found in the toxicological effects on cell viability of ultra violet irradiated anTiO$_2$ and rnTiO$_2$. In conclusion, our results indicate that anTiO$_2$ is less potent in induction of alveolar macrophage infiltration, 8-OHdG and MIP1α expression in the lung, and growth stimulation of A549 cells *in vitro* than rnTiO$_2$.

Keywords: Nanosized titanium dioxide - anatase - rutile - lung toxicity - MIP1α

Introduction

There are three mineral forms of natural titanium dioxide particles: rutile, anatase and brookite. Engineered anatase and rutile nanosized titanium dioxide particles (anTiO$_2$ and rnTiO$_2$) are being manufactured in large quantities worldwide and applied in many fields including material industry, electronic industry, commercial products and biosystems. Due to differences in crystal structure, anTiO$_2$ has better photocatalytic activity than rnTiO$_2$ (Kakinoki et al., 2004). Accordingly, anTiO$_2$ is mainly used in paints, such as surface painting of the walls and windows of buildings and vehicles, and photocatalytic systems, while rnTiO$_2$ is preferentially used in cosmetics, sunscreen and food additives.

Large quantity production and widespread application of nTiO$_2$ have given rise to concern about its health and environmental effects. Anatase and rutile type titanium dioxide particles, nanosized and larger, are evaluated as Group 2B carcinogens (possibly carcinogenic to humans) by WHO/International Agency for Research on Cancer (IARC, 2010), based on 2-year animal aerosol inhalation studies (Mohr et al., 2006). Pulmonary exposure to rnTiO$_2$ promotes DHPN-induced lung carcinogenesis in rats, and the promotion effect is possibly associated with rnTiO$_2$ burdened alveolar macrophage derived macrophage inflammatory protein 1 alpha (MIP1α), which acts as a growth factor to stimulate the proliferation of human lung adenocarcinoma cells (A549) *in vitro* (Xu et al., 2010). Dermal application of anTiO$_2$ has been shown to cause significant increases in the level of superoxide dismutase and malondialdehyde in hairless mice (Wu et al., 2009).

Size and photoactivation affect the *in vitro* toxicity of anTiO$_2$ and rnTiO$_2$. anTiO$_2$ (10 and 20 nm) induces

[1]*Department of Molecular Toxicology, Nagoya City University Graduate School of Medical Sciences and Medical School,*[2]*Laboratory of Nanotoxicology Project, Nagoya City University, Nagoya,* [3]*DIMS Institute of Medical Science, Aichi,* [4]*National Institute of Health Sciences, Tokyo, Japan* *For correspondence: suzui@med.nagoya-cu.ac.jp*

oxidative DNA damage, lipid peroxidation and micronuclei formation, and increases hydrogen peroxide and nitric oxide production in BEAS-2B cells, a human bronchial epithelial cell line, but anTiO$_2$ 200 nm particles do not (Gurr et al., 2005). In contrast, both nano-sized and 200nm ruTiO$_2$ are toxic *in vitro* (Gurr et al., 2005; Sayes et al., 2006). On the other hand, under ultraviolet irradiation, anTiO$_2$ is 100 times more toxic to human dermal fibroblasts and A549 cells than rnTiO$_2$, and is more potent than rnTiO$_2$ in the induction of lactate dehydrogenase release, reactive oxygen species production and interleukin 8 secretion (Sayes et al., 2006). Experimental data demonstrating differences in the toxic effects of anTiO$_2$ and rnTiO$_2$ *in vivo*, however, are still lacking.

Respiratory exposure to nTiO$_2$ particles can occur both at the workplace, e.g., in manufacturing and packing sites, and outside the workplace during their use (Maynard et al., 2006; Schulte et al., 2008). In the present study, we delivered anTiO$_2$ and rnTiO$_2$ to the rat lung by trans-tracheal intra-pulmonary spraying (TIPS) and compared lung inflammation and several toxicological parameters induced by anTiO$_2$ and rnTiO$_2$. The results indicated that obvious lung inflammatory lesions were not observed in the rats, and anTiO$_2$ or rnTiO$_2$ particles were phagocytosed by alveolar macrophages. Analysis of alveolar macrophage induction, 8-OHdG level in the lung, and MIP1α expression both *in vivo* in the lung and *in vitro* in PAM indicated that anTiO$_2$ elicited lower levels of biological responses than rnTiO$_2$. Long-term toxic effects of anTiO$_2$ and rnTiO$_2$ still need to be clarified.

Materials and Methods

Preparation and characterization of nTiO$_2$ suspension

Nanosized TiO$_2$ particles (anatase type without coating, primary size 25 nm and rutile type without coating, primary size 20 nm) were provided by Japan Cosmetic Association, Tokyo, Japan. Both anTiO$_2$ and rnTiO$_2$ particles were suspended in saline at 500 μg/ml and then autoclaved. The suspensions were sonicated for 20 min shortly before use to prevent aggregate formation.

Characterization of nTiO$_2$ was conducted as follows: The shapes of nTiO$_2$ in suspension were imaged by transmission electron microscopy (TEM) and scanning electron microscopy (SEM). Element analysis was performed by a an X-ray microanalyzer (EDAX, Tokyo, Japan), after aliquots of nTiO$_2$ were loaded onto a carbon sheet. For size distribution analysis, aliquots of the 500 μg/ml nTiO$_2$ suspension were loaded onto clean glass slides and photographed under a polarized light microscope (Olympus BX51N-31P-O polarized light microscope, Tokyo, Japan), and the photos were then analyzed by an image analyzer system (IPAP, Sumika Technos Corporation, Osaka, Japan). Over 1000 particles of anTiO$_2$ and rnTiO$_2$ were measured.

Animals

Female Sprague-Dawley rats (SD rats) were purchased from CLEA Japan Co., Ltd (Tokyo, Japan). The animals were housed in the animal center of Nagoya City University Medical School, maintained on a 12 hour light-dark cycle and received oriental MF basal diet (Oriental Yeast Co., Tokyo, Japan) and water *ad lib*. The research was conducted according to the Guidelines for the Care and Use of Laboratory Animals of Nagoya City University Medical School and the experimental protocol was approved by the Institutional Animal Care and Use Committee (H22M-19).

Trans-tracheal intra-pulmonary spraying (TIPS) protocol

Three groups of 6 female SD rats (Group 1, saline; Group 2, anTiO$_2$; and Group 3, rnTiO$_2$) aged 9 weeks were acclimated for 7 days prior to the start of the study. Saline and nTiO$_2$ suspensions were administered by TIPS to the animals under isoflurane anesthesia: The nozzle of a Microsprayer (series IA-1B Intratracheal Aerosolizer, Penn-century, Philadelphia, PA) connected to a 1 ml syringe was inserted into the trachea through the larynx and a total volume of 0.5 ml suspension was sprayed into the lungs synchronizing with spontaneous inspiration by the animal (Xu et al., 2010). Rats were treated once every the other day over a 2 week period, a total of eight treatments. The total amount of anTiO$_2$and rnTiO$_2$ administered to Groups 2 and 3 was 2.0 mg per rat. Six hours after the last spraying, the animals were killed and the whole lung was excised and divided into two parts; the left lung was cut into pieces and immediately frozen at -80°C and used for biochemical analysis, and the right lung was fixed in 4% paraformaldehyde solution in phosphate-buffered saline (PBS) adjusted to pH 7.3 and processed for immunohistochemical, light microscopic and transmission electron microscopic (TEM) examinations.

Light microscopy and transmission electron microscopy

Hematoxylin and eosin (H&E) stained sections were used for pathological observation. The number of alveolar macrophages in H&E lung tissue slides was counted and expressed as number per mm^2.

Slides were observed under light microscopic observation, the corresponding area in the paraffin block was cut out, deparaffinized and embedded in epoxy resin and processed for TEM and titanium element analysis with a JEM-1010 transmission electron microscope (JEOL Co. Ltd, Tokyo, Japan) equipped with an X-ray microanalyzer (EDAX, Tokyo, Japan).

Analysis of 8-hydroxydeoxy guanosine levels

For the analysis of 8-hydroxydeoxyguanosine (8-OHdG) levels, genomic DNA was isolated from a piece of the left lung with a DNA Extractor WB kit (Wako Chemicals Co. Ltd). 8-OHdG levels were determined with an 8-OHdG ELISA Check kit (Japan Institute for Control of Aging, Shizuoka, Japan).

RNA isolation, cDNA synthesis and RT-PCR analysis of gene expression

Pieces of the left lungs (50-100 mg) were thawed, rinsed 3 times with ice cold PBS, and total RNA was isolated using 1 ml Trizol Reagent (Invitrogen, Karlsruhe, Germany). For reverse transcription PCR (RT-PCR) and real-time PCR, first strand cDNA synthesis from 2 mg of total RNA was performed using SuperScript™ III First-Strand Synthesis

System (Invitrogen of Life Technologies, CA) according to the manufacturer's instructions. PCR primers for rat MIP1α were 5'-TTTTGAGACCAGCAGCCTTT -3' (forward) and 5'- CTCAAGCCCCTGCTCTACAC-3' (reverse), and the product size was 191bp. b-actin was used as internal control and the primers were 5'- AGCCATGTACGTAGCCATCC-3' (forward) and 5'-CTCTCAGCTGTGGTGGTGAA-3', and the product size was 228 bp. RT-PCR was conducted using an iCycler (BioRad Life Sciences, CA) as follows: 95°C 20 sec, 60°C 20 sec, 72°C 30sec, 30 cycles for MIP1α; and 95°C 20 sec, 60°C 20 sec, 72°C 30sec, 15 cycles for b-actin. Real-time PCR analysis of MIP1α gene expression was performed with a 7300 Real Time PCR System (Applied Biosystem, CA) using Power SYBR Green PCR Master Mix (Applied Biosystem, CA) according to the manufacturer's instructions. b-actin gene was used as the normalizing reference gene.

Immunohistochemical analysis

Paraffin embedded lung tissues sections were immunostained with polyclonal anti-rat MIP1α (BioVision, Lyon, France). Antigen retrieval was carried out by microwave for 20 min in 10 mmol/L citrate buffer (pH 6.0). Antibody was diluted 1:100 in blocking solution and applied to the slides, and the slides were incubated at 4°C overnight. Immunohistochemical staining was done by the avidin-biotin complex method (ABC) using the Vectastain Elite ABC system (Vector Laboratories, Burlingame, CA). Biotinylated goat anti-rabbit IgG (Vector Laboratories) was used as a secondary antibody at a dilution of 1:500 for 1 hour and visualized using avidin-conjugated alkaline phosphatase complex (ABC kit, Vector laboratories) and Alkaline Phosphatase Substrate Kit (Vector Laboratories). Sections were lightly counterstained with hematoxylin for microscopic examination.

ELISA for MIP1α in the lung tissues and the supernatants of cell culture

Left lung tissue samples (50-100mg) were thawed, rinsed 3 times with ice cold PBS and homogenized in 1 ml of tissue extraction reagent (PeproTech, London, UK) containing 1% (v/v) Proteinase Inhibitor Cocktail (Sigma-Aldrich, St Louis, MO, USA). The homogenates were clarified by centrifugation at 10,000g, 4°C for 5 min. The protein content in the supernatants was measured with a BCATM Protein assay kit (Pierce). The levels of MIP1α in the supernatants were measured using rat MIP1α ELISA Development Kit (Cat#: 900-K75, Peprotech, Inc., Rocky Hill, NJ.) according to the manufacturer's instruction, and expressed as pg/mg lung tissue protein. The levels of MIP1α in cell culture supernatants were measured as described above and expressed as pg/ml.

Isolation of PAM and exposure of nTiO$_2$ to PAM cells

Induction and isolation of alveolar macrophages in female SD rats was performed as described previously (Xu et al., 2010). 10^6 primary alveolar macrophages (PAM) were cultured in RPMI1640 containing 2% fetal bovine serum and antibiotics overnight at 37°C, 5% CO$_2$. 500 μg/ml of anTiO$_2$ and rnTiO$_2$ suspensions was then added

to the cultures to a final concentration of 10 μg/ml and the cells were incubated for another 24 hours. RNA was isolated from the PAM and the level of MIP1α protein in the conditioned culture media was measured by ELISA.

In vitro cell proliferation assay

A549 cells were seeded into 96-well culture plates at 2×10^3 cells per well in 2% fetal bovine serum Dulbecco's modified Eagle's medium (Wako Chemicals Co., Ltd). After overnight incubation, the medium was replaced with the conditioned PAM culture media treated with anTiO$_2$ or rnTiO$_2$, and the cells were incubated for another 72 hours, with or without 20 μg/ml of anti-MIP1α neutralizing antibody (R&D Systems, Minneapolis, MN). The relative cell number of A549 cells was determined using a Cell counting Kit-8 (Dojindo Molecular Technologies, Rockville, MD) according to the manufacturer's instruction.

Cytotoxicity assay in vitro

A549 cells, the primary human lung fibroblast cell line CCD34 (ECACC, Cat. No. 90110514) and PAM were used for cytotoxicity analyses. Cells were seeded in 96 well plates at 5×10^3/well and incubated overnight. The cells were then treated with anTiO$_2$ and rnTiO$_2$ suspensions at final concentrations of 0, 2, 10, or 50 μg/ml and then incubated for another 24 hours. The relative cell number was determined as described above.

Cytotoxicity of anTiO$_2$ and rnTiO$_2$ under ultraviolet B irradiation

A549 cells were used for analysis of nTiO$_2$ cytotoxicity under ultraviolet irradiation. First, we determined an irradiation time that did not affect the cell viability as follows: A549 cells were seeded into 96 well plates at 1×10^3/well in 200 μL Dulbecco's modified Eagle's medium (Wako Chemicals Co., Ltd) containing 10% fetal bovine serum and incubated overnight. The cells were irradiated with ultraviolet B (UVB) for 0, 30 sec, 1 min, 2 min, 5 min and 10 min with a transilluminator (Vilber Lourmat, France). The light intensity was 1000 mW/cm^2, and the emission spectrum was from 270 nm to 330 nm with a peak at 312 nm. The non-irradiated control wells were covered with a sterile aluminium sheet to prevent irradiation. The relative cell number was determined after incubation for 48 hours at 37°C, 5% CO$_2$.

Next, we observed the effect of anTiO$_2$ and rnTiO$_2$ on cell viability under UVB. A549 cells were seeded into 96 well plate at 1×10^3well in 100 μL culture media and incubated overnight. Then, 100 mL of anTiO$_2$ or rnTiO$_2$ suspensions in DMEM culture medium containing 10% FBS was added into the wells to final concentration of 0, 2, 5 and 10 μg/ml and incubated for 30 min. The cells were irradiated with UVB for 2 min (2 min UVB irradiation did not affect cell viability), and incubated for another 48 hours, before determination of relative cell number.

Statistical and analysis

Statistical significance of the *in vitro* and *in vivo* findings was analyzed using the two-tailed Student's t-test. *In vitro* and *in vivo* data are presented as means±standard

deviations. A value of p<0.05 was considered to be significant.

Results

Characterization of nTiO₂ particles in suspension

TEM images showed that individual anTiO$_2$ particles were spherical in shape, while individual rnTiO$_2$ particles had a rod-like shape, and both anTiO$_2$ and rnTiO$_2$ formed large aggregates in suspension (Figure. 1A and B). Similarly, SEM observation indicated aggregate formation of both types of nTiO$_2$ particles (Figure. 1C and D). Peaks of titanium (green arrows) and oxygen (blue arrows), which are present in both types of nTiO$_2$ particles, and carbon (white arrows) and nitrogen (red arrow), which are present in the carbon sheets used in the SEM, were observed by elemental scanning (Figure. 1E and F). Peaks of other elements were not detected in either the rnTiO$_2$ or anTiO$_2$ samples. Analyses of particle size showed that the mean and medium diameters were 5.491±2.727 mm and 5.127 mm for anTiO$_2$, and 3.799±2.231 mm and 3.491 mm for rnTiO$_2$ (Figure. 1G), confirming aggregate formation of both types of nTiO$_2$ particles in suspension.
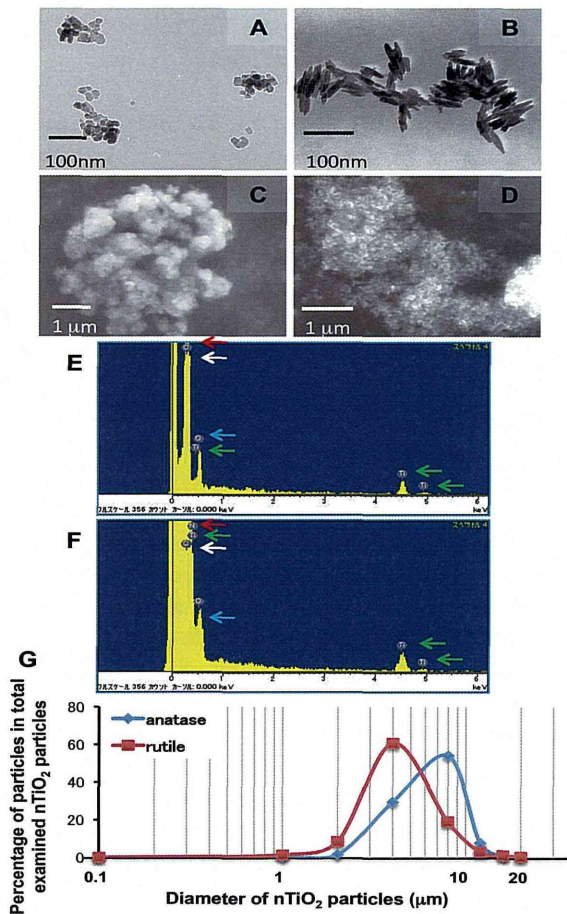
Figure 1. Characterization of nTiO₂ Particles in Suspension. A and B: TEM imagines of anTiO$_2$ and rnTiO$_2$ particles in suspension. C and D: SEM images of anTiO$_2$ and rnTiO$_2$ particles. E and F: Element scanning showed peaks of titanium (green arrows), oxygen (blue arrows), carbon (white arrows) and nitrogen (red arrows) in anTiO$_2$ and rnTiO$_2$ particles. G: Size distribution of anTiO$_2$ and rnTiO$_2$ in suspension

Histological observation and 8-OHdG level in the lung tissue

Only a few small lung inflammatory lesions were observed in rats treated with anTiO$_2$ and rnTiO$_2$ (Figure. 2A, B and C). Alveolar macrophage infiltration was found throughout the lung tissue, and most of the alveolar macrophages were seen with phagocytosed anTiO$_2$ particles or rnTiO$_2$ particles (Figure. 2D, E an F). TEM observation demonstrated that both anTiO$_2$ and rnTiO$_2$ were deposited in various sizes in the cytoplasm of the alveolar macrophages (Figure. 2G and H). Neither anTiO$_2$ or rnTiO$_2$ particles were found in other types of cells in the lung tissue. The number of macrophages per mm^2 lung tissue section was 67.1±15.8 (saline), 165.0±34.9 (anTiO$_2$) and 214.2±44.1 (rnTiO$_2$). The numbers of macrophages in the anTiO$_2$ and rnTiO$_2$ treated groups was significantly higher than in the control group (p<0.001), and the anTiO$_2$ treated group had lower macrophage infiltration than the rnTiO$_2$ treated group.

The level of 8-OHdG, a parameter of oxidative DNA damage caused by reactive oxygen species (ROS), in the lung tissue in rats treated with anTiO$_2$ and rnTiO$_2$ was 1.96±0.77 and 3.07±1.25 (pg per mg DNA), respectively, and was higher than that of the control (1.44±0.63): The increase in 8-OHdG in the lungs of rnTiO$_2$, but not anTiO$_2$, treated rats was significantly higher than the control
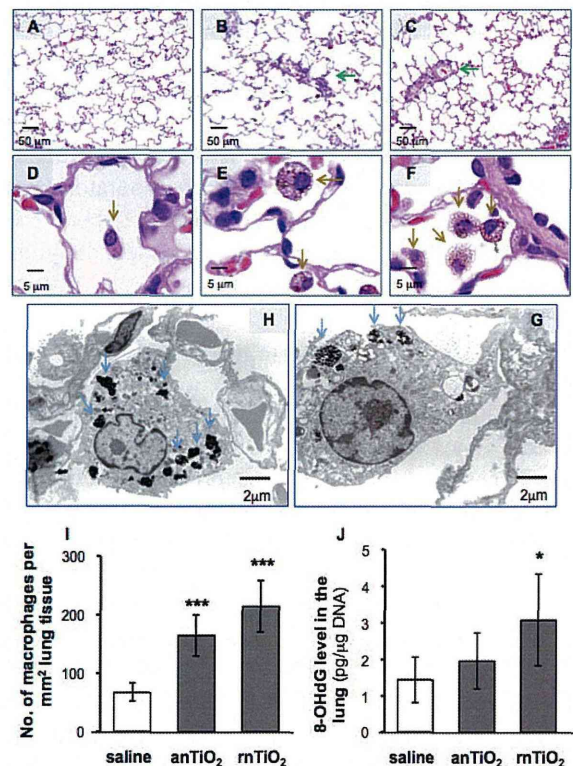
Figure 2. Histological Observation and 8-OHdG Level in the Lung Tissue. A, B and C: Histological imagines of lung tissue treated with saline, anTiO$_2$ and rnTiO$_2$, respectively. Green arrows indicate small inflammatory lesions. D (saline), E (anTiO$_2$) and F (rnTiO$_2$): Higher magnification imagines of alveolar macrophages (brown arrows). nTiO$_2$ particles are clearly observed. G and H: TEM imagines of alveolar macrophages with anTiO$_2$ and rnTiO$_2$ particles in their cytoplasm (blue arrows). I and J: The numbers of alveolar macrophages and 8-OHdG levels in the lung tissue. *, *** represent p<0.05 and 0.001, respectively, versus saline

(p<0.05) (Figure. 2J).

### MIP1α expression in the lung tissue

RT-PCR suggested an increase in MIP1α mRNA expression in lung tissue treated with anTiO$_2$ or rnTiO$_2$ (Figure. 3A). Real-time PCR analysis indicated that compared with the control group, the increase was 2.79-fold for anTiO$_2$ and 5.35-fold for rnTiO$_2$. MIP1α mRNA expression was also significantly lower in the anTiO$_2$ treated group compared to the rnTiO$_2$ treated group (Figure. 3B). The levels of MIP1α protein in the lung tissue were 32.8±0.31 and 52.7±0.58 pg/mg lung protein in the anTiO$_2$ and rnTiO$_2$ treated groups, both significantly higher than that of the control group (20.8±0.24) (Figure. 3C). Similarly to MIP1α mRNA expression, MIP1α protein expression was significantly lower in the anTiO$_2$ treated group compared to the rnTiO$_2$ treated group.

To find out what cells in the lung accounted for the increased MIP1α protein expression, we examined tissue samples using MIP1α immunohistochemistry. As shown in Figure. 3D, E and F, MIP1α protein was produced by anTiO$_2$ or anTiO$_2$ burdened alveolar macrophages.

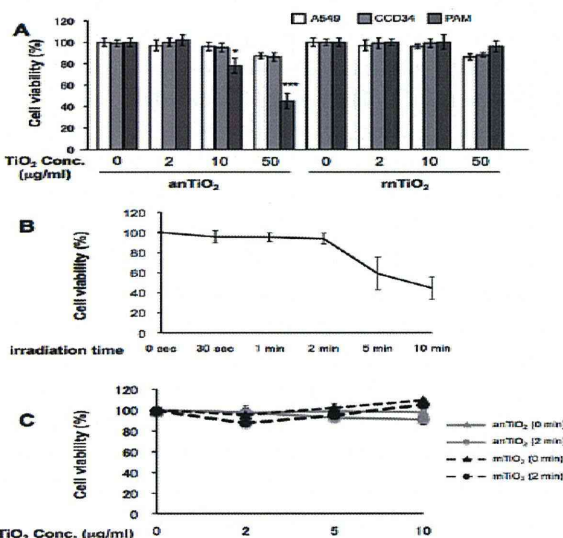### Exposure of PAMs to anTiO$_2$ and rnTiO$_2$ and cell proliferation assays in vitro

As in the lung tissue, in vitro exposure of PAM to nTiO$_2$ induced expression of MIP1α mRNA (Figure. 4A) and protein (Figure. 4B). Treatment with anTiO$_2$ and rnTiO$_2$ caused 11.96-fold and 15.26-fold increases in the expression of MIP1α mRNA, respectively, in cultured PAM. The level of MIP1α protein in the cell culture medium was 32.8±1.1 pg/mL for anTiO$_2$ and 52.7±1.3 pg/mL for rnTiO$_2$, significantly higher than that of the control
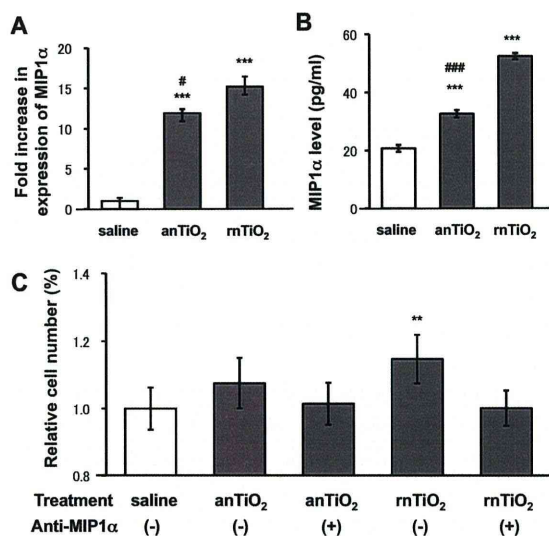
Figure 4. The Effect of anTiO$_2$ and rnTiO$_2$ on PAM Cells. The expression of MIP1α mRNA in cultured PAM (A) and protein in the culture media (B) indicate that treatment with anTiO$_2$ or rnTiO$_2$ increased MIP1α expression in the PAM. Conditioned cell culture media of PAM treated with rnTiO$_2$, but not anTiO$_2$, had a significant effect on proliferation of A549 cells, and this promotion was attenuated by addition of 20 µg/ml MIP1α neutralizing antibody (C). **, ***represent p<0.01 and 0.001, versus saline; #, ###represent p<0.05 and 0.001, versus rnTiO$_2$

Figure 5. In vitro Assays. A: The effect of anTiO$_2$ and rnTiO$_2$ on the viability of A549, CCD34 and PAM cells. B: The effect of UVB irradiation on the viability of A549 cells. C: The effect of anTiO$_2$ and rnTiO$_2$ on the vi ability of A549 under UVB irradiation. *, *** represent p<0.05 and 0.001, versus the vehicle

Figure 3. Expression of MIP1α in the Lung Tissue. A, B and C: Analysis of expression of MIP1α mRNA by RT-PCR (A) and real-time PCR (B) and protein by ELISA (C). D, E, and F: Immunohistochemistry shows MIP1α expressed in alveolar macrophages of lung tissue treated with saline (D), anTiO$_2$ (E) and rnTiO$_2$ (F). *, *** represent p<0.05 and 0.001, respectively, versus saline; ### represent p<0.001, versus rnTiO$_2$

(20.8±1.2 pg/mL). Both mRNA and protein expression of MIP1α was significantly lower in the anTiO$_2$ treated PAM compared to the rnTiO$_2$ treated cells.

The supernatants of the culture media of PAM treated with anTiO$_2$ showed only a tendency to increase A549 cell proliferation, while those collected from PAM treated with rnTiO$_2$ significantly promoted proliferation of A549 cells (115%) compared to supernatants from the saline treated group (Figure. 4C). The promotion effect of the supernatants of PAM cell cultures treated with anTiO$_2$ or

Takamasa Numano et al

rnTiO$_2$ was attenuated by anti-MIP1α neutralizing antibodies, indicating MIP1α is probably a mediator of the increase in A549 cell proliferation.

In vitro cytotoxicity assays

In vitro cytotoxicity assays indicated that both anTiO$_2$ and rnTiO$_2$ had little effect on the cell viability of A549 and CCD34 cells at a concentration of up to 50 mg/ml. anTiO$_2$ had a cytotoxic effect on the cell viability of PAM at doses of 10 and 50 mg/ml, while rnTiO$_2$ did not impair the cell viability of PAM at any of the examined concentrations (Figure. 5A).

To investigate whether UVB irradiation affected the cytotoxic effects of anTiO$_2$ and rnTiO$_2$ on cell viability, we first determined the exposure times that ultraviolet B irradiation itself did not impair the viability of A549 cells. As shown in Figure. 5B, irradiation for up to 2 min did not have any effect on the viability of A549 cells. With 2 min of UVB irradiation, neither anTiO$_2$ or rnTiO$_2$ at doses of 2, 5 or 10 μg/ml resulted in any decrease in the viability of A549 cells (Figure. 5C).

Discussion

The toxicity of nanoparticles usually includes tiers of biological responses such as induction of ROS and inflammation (Nel et al., 2006). This may contribute to carcinogenic potential (Tsuda et al., 2009). Thus, in the present study, we compared several parameters ofr inflammation and oxidative stress induced by TIPS of anTiO$_2$ and rnTiO$_2$. The results indicated that both anTiO$_2$ and rnTiO$_2$ particles were phagocytosed by alveolar macrophages and did not cause strong lung inflammation. Treatment with anTiO$_2$ and rnTiO$_2$ increased alveolar macrophage infiltration, MIP1α expression and 8-OHdG production: anTiO$_2$ had less effect than rnTiO$_2$.

Phagocytosis by alveolar macrophages is a major defense mechanism for deposition and clearance of inhaled particles (Heppleston, 1984; Rom et al., 1991; Geiser et al., 2008). However, activation of alveolar macrophages is strongly associated with inflammatory reactions and ROS production (Renwick et al., 2001; Bhatt et al., 2002; Wang et al., 2007). Also, MIP1α, secreted from rnTiO$_2$ burden alveolar macrophages, is possibly involved in the promotion of lung carcinogenesis (Xu et al., 2010). Similarly, pleural macrophage recruitment and activation are involved in the pathogenesis of asbestos (Choe et al., 1997). These results indicate two contrasting roles of alveolar macrophages in pathogenesis and host defense.

The toxic effects of nanoparticles are dependent on their size, shape, surface functionality and composition (Albanese et al., 2012). In the present study, we used comparable sizes of anTiO$_2$ and rnTiO$_2$ particles. Both types of nTiO$_2$ had no surface coating and had no obvious difference in elemental composition. Therefore, differences in alveolar macrophage induction, MIP1α expression and 8-OHdG production between anTiO$_2$ and rnTiO$_2$ are likely due to their different crystal structures and shapes. The lower toxicity of anTiO$_2$ compared to rnTiO$_2$ in the absence of UVB irradiation in our study

is consistent with a previous *in vitro* study with bulk rutile and anatase TiO$_2$ (Gurr et al., 2005). In contrast to a previous study (Sayes et al., 2006), in the present study anTiO$_2$ and rnTiO$_2$ did not exhibit different toxicities on the cell viability of A549 cells under ultraviolet irradiation.

It should be noted that both types of anTiO$_2$ and rnTiO$_2$ particles formed aggregates in suspension, and aggregation may alter their bio-reactivity. Whether anTiO$_2$ and rnTiO$_2$ particles have different long-term effects remains to be clarified.

In conclusion, *in vivo* exposure of the rat lung to anTiO$_2$ or rnTiO$_2$ particles increased alveolar macrophage infiltration, MIP1α expression and 8-OHdG production, with anTiO$_2$ eliciting lower levels of biological responses than rnTiO$_2$. Similarly, exposure of primary alveolar macrophages to rnTiO$_2$ *in vitro* resulted the cells producing more MIP1α mRNA and protein than cells exposed to anTiO$_2$. Cytotoxicity assays *in vitro* indicated that both anTiO$_2$ and rnTiO$_2$ had very low cellular toxicity even under UVB irradiation.

Acknowledgements

References

Albanese A, Tang PS, Chan WC (2012). The effect of nanoparticle size, shape, and surface chemistry on biological systems. *Annu Rev Biomed Eng*, **14**, 1-16.

Bhatt NY, Kelley TW, Khramtsov VV, et al (2002). Macrophage-colony-stimulating factor-induced activation of extracellular-regulated kinase involves phosphatidylinositol 3-kinase and reactive oxygen species in human monocytes. *J Immunol*, **169**, 6427-34.

Choe N, Tanaka S, Xia W, et al (1997). Pleural macrophage recruitment and activation in asbestos-induced pleural injury. *Environ Health Perspect*, **105**, 1257-60.

Geiser M, Casaulta M, Kupferschmid B, et al (2008). The role of macrophages in the clearance of inhaled ultrafine titanium dioxide particles. *Am J Respir Cell Mol Biol*, **38**, 371-6.

Gurr JR, Wang AS, Chen CH, et al (2005). Ultrafine titanium dioxide particles in the absence of photoactivation can induce oxidative damage to human bronchial epithelial cells. *Toxicology*, **213**, 66-73.

Heppleston AG (1984). Pulmonary toxicology of silica, coal and asbestos. *Environ Health Perspect*, **55**, 111-27.

IARC (2010). Carbon black, titanium dioxide, and talc. *IARC Monogr Eval Carcinog Risks Hum*, **93**, 1-413.

Kakinoki K, Yamane K, Teraoka R, et al (2004). Effect of relative humidity on the photocatalytic activity of titanium dioxide and photostability of famotidine. *J Pharm Sci*, **93**, 582-9.

Maynard AD, Aitken RJ, Butz T, et al (2006). Safe handling of nanotechnology. *Nature*, **444**, 267-9.

Mohr U, Ernst H, Roller M, et al (2006). Pulmonary tumor types induced in Wistar rats of the so-called "19-dust study". *Exp Toxicol Pathol*, **58**, 13-20.

Nel A, Xia T, Madler L, et al (2006). Toxic potential of materials at the nanolevel. *Science*, **311**, 622-7.

Renwick LC, Donaldson K, Clouter A (2001). Impairment of alveolar macrophage phagocytosis by ultrafine particles.

Toxicol Appl Pharmacol, **172**, 119-27.

Rom WN, Travis WD, Brody AR (1991). Cellular and molecular basis of the asbestos-related diseases. *Am Rev Respir Dis*, **143**, 408-22.

Sayes CM, Wahi R, Kurian PA, et al (2006). Correlating nanoscale titania structure with toxicity: a cytotoxicity and inflammatory response study with human dermal fibroblasts and human lung epithelial cells. *Toxicol Sci*, **92**, 174-85.

Schulte P, Geraci C, Zumwalde R, et al (2008). Occupational risk management of engineered nanoparticles. *J Occup Environ Hyg*, **5**, 239-49.

Tsuda H, Xu J, Sakai Y, Futakuchi M, Fukamachi K (2009). Toxicology of engineered nanomaterials - A review of carcinogenic potential. *Asian Pac J Cancer Prev*, **10**, 975-980.

Wang H, Li J, Quan X, et al (2007). Formation of hydrogen peroxide and degradation of phenol in synergistic system of pulsed corona discharge combined with TiO_2 photocatalysis. *J Hazard Mater*, **141**, 336-43.

Wu J, Liu W, Xue C, et al (2009). Toxicity and penetration of TiO_2 nanoparticles in hairless mice and porcine skin after subchronic dermal exposure. *Toxicol Lett*, **191**, 1-8.

Xu J, Futakuchi M, Iigo M, et al (2010). Involvement of macrophage inflammatory protein 1alpha (MIP1alpha) in promotion of rat lung and mammary carcinogenic activity of nanoscale titanium dioxide particles administered by intra-pulmonary spraying. *Carcinogenesis*, **31**, 927-35.